

# 3D-Aware Object Goal Navigation via Simultaneous Exploration and Identification

Jiazhao Zhang<sup>1,2,\*</sup>Liu Dai<sup>3,\*</sup>Fanpeng Meng<sup>4</sup>Qingnan Fan<sup>5</sup>Xuelin Chen<sup>5</sup>Kai Xu<sup>6</sup>He Wang<sup>1†</sup><sup>1</sup> CFCS, Peking University    <sup>2</sup> Beijing Academy of Artificial Intelligence    <sup>3</sup>CEIE, Tongji University<sup>4</sup>Huazhong University of Science and Technology    <sup>5</sup>Tencent AI Lab    <sup>6</sup>National University of Defense Technology

## Abstract

*Object goal navigation (ObjectNav) in unseen environments is a fundamental task for Embodied AI. Agents in existing works learn ObjectNav policies based on 2D maps, scene graphs, or image sequences. Considering this task happens in 3D space, a 3D-aware agent can advance its ObjectNav capability via learning from fine-grained spatial information. However, leveraging 3D scene representation can be prohibitively unpractical for policy learning in this floor-level task, due to low sample efficiency and expensive computational cost. In this work, we propose a framework for the challenging 3D-aware ObjectNav based on two straightforward sub-policies. The two sub-polices, namely corner-guided exploration policy and category-aware identification policy, simultaneously perform by utilizing online fused 3D points as observation. Through extensive experiments, we show that this framework can dramatically improve the performance in ObjectNav through learning from 3D scene representation. Our framework achieves the best performance among all modular-based methods on the Matterport3D and Gibson datasets, while requiring (up to 30x) less computational cost for training. The code will be released to benefit the community.<sup>1</sup>*

## 1. Introduction

As a vital task for intelligent embodied agents, object goal navigation (ObjectNav) [38, 49] requires an agent to find an object of a particular category in an unseen and unmapped scene. Existing works tackle this task through end-to-end reinforcement learning (RL) [27, 36, 47, 51] or modular-based methods [9, 14, 35]. End-to-end RL based methods take as input the image sequences and directly output low-level navigation actions, achieving competitive

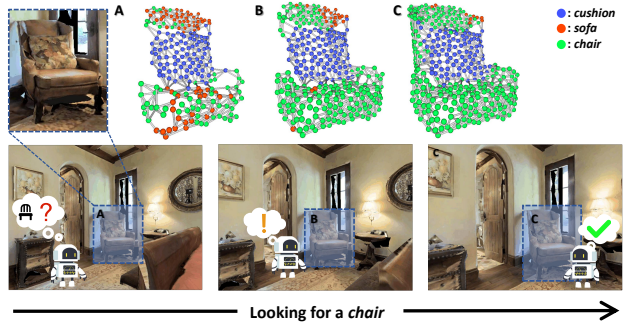
<sup>\*</sup>Joint first authors<sup>†</sup>Corresponding author: [hewang@pku.edu.cn](mailto:hewang@pku.edu.cn)<sup>1</sup>Homepage: <https://pku-epic.github.io/3D-Aware-ObjectNav/>

Figure 1. We present a 3D-aware ObjectNav framework along with simultaneous exploration and identification policies: **A**→**B**, the agent was guided by an exploration policy to look for its target; **B**→**C**, the agent consistently identified a target object and finally called STOP.

performance while suffering from lower sample efficiency and poor generalizability across datasets [3, 27]. Therefore, we favor modular-based methods, which usually contain the following modules: a semantic scene mapping module that aggregates the RGBD observations and the outputs from semantic segmentation networks to form a semantic scene map; an RL-based goal policy module that takes as input the semantic scene map and learns to online update a goal location; finally, a local path planning module that drives the agent to that goal. Under this design, the semantic accuracy and geometric structure of the scene map are crucial to the success of object goal navigation.

We observe that the existing modular-based methods mainly construct 2D maps [8, 9], scene graphs [34, 56] or neural fields [43] as their scene maps. Given that objects lie in 3D space, these scene maps are inevitably deficient in leveraging 3D spatial information of the environment comprehensively and thus have been a bottleneck for further improving object goal navigation. In contrast, forming a 3D scene representation naturally offers more accurate, spatially dense and consistent semantic predictions than its 2D counterpart, as proved by [12, 31, 45]. Hence, if the agent could take advantage of the 3D scene understanding and

form a 3D semantic scene map, it is expected to advance the performance of ObjectNav.

However, leveraging 3D scene representation would bring great challenges to ObjectNav policy learning. First, building and querying fine-grained 3D representation across a floor-level scene requires extensive computational cost, which can significantly slow down the training of RL [7,55]. Also, 3D scene representation induces considerably more complex and high-dimensional observations to the goal policy than its 2D counterpart, leading to a lower sample efficiency and hampering the navigation policy learning [22, 57]. As a result, it is demanding to design a framework to efficiently and effectively leverage powerful 3D information for ObjectNav.

To tackle these challenges, we propose a novel framework composed of an online semantic point fusion module for 3D semantic scene mapping and two parallel policy networks in charge of scene exploration and object identification, along with a local path planning module. Our online semantic point fusion module extends a highly efficient online point construction algorithm [53] to enable online semantic fusion and spatial semantic consistency computation from captured RGBD sequences. This 3D scene construction empowers a comprehensive 3D scene understanding for ObjectNav. Moreover, compared to dense voxel-based methods [7, 55], our point-based fusion algorithm are more memory-efficient [40, 46] which makes it practically usable for floor-level navigation task. (See Figure 1)

Moreover, to ease the learning of navigation policy, we further propose to factorize the navigation policy into two sub-policies, namely exploration and identification. The two policies simultaneously perform to roll out an exploration goal and an identified object goal (if exist), respectively. Then the input for the local path planning module will switch between these two goals, depending on whether there exists an identified target object. More specifically, we propose a corner-guided exploration policy which learns to predict a long-term discrete goal at one of the four corners of the bounding box of the scene. These corner goals efficiently drive the agent to perceive the surroundings and explore regions where the target object is possibly settled. And for identification, a category-aware identification policy is proposed to dynamically learn a discrete confidence threshold to identify the semantic predictions for each category. Both of these policies are trained by RL in low-dimensional discrete action space. Through experiments, the simultaneous two-policy mechanism and discrete action space design dramatically reduce the difficulty in learning for 3D-aware ObjectNav and achieve better performance than existing modular-based navigation strategies [26, 35].

Through extensive evaluation on the public benchmarks, we demonstrate that our method performs online 3D-aware

ObjectNav at 15 FPS while achieving the state-of-the-art performance on navigation efficiency. Moreover, our method outperforms all other modular-based methods in both efficiency and success rate with up to 30x times less computational cost.

Our main contributions include:

- We present the first 3D-aware framework for ObjectNav task.
- We build an online point-based construction and fusion algorithm for efficient and comprehensive understanding of floor-level 3D scene representation.
- We propose a simultaneous two-policy mechanism which mitigates the problem of low sample efficiency in 3D-aware ObjectNav policy learning.

## 2. Related Work

**GoalNav with Visual Sequences.** There are constantly emerging researches on object goal navigation. One line of recent works directly leverages RGBD sequences, called end-to-end RL methods [47], which tends to implicitly encode the environment and predict low-level actions. These works benefit from visual representation [29, 50], auxiliary task [51], and data augmentation [27], demonstrating strong results on object goal navigation benchmarks [1, 49]. However, aiming to learn all skills through one policy from scratch, e.g., avoiding collisions, exploration, and stopping, it's well known that end-to-end RL methods suffer from low sampling efficiency for training and limited generalizability when transferred to the real world [3, 35]. Instead, our work uses explicit map to represent the environment, which ensures our sample efficiency and also obtain more generalizability through a modular-based paradigm [1, 35].

**GoalNav with Explicit Scene Representations.** To ease the burden of learning directly from visual sequences, another category of methods, called modular-based methods [8, 9, 15, 17, 32], use explicit representations as a proxy for robot observations. By leveraging explicit scene representations like scene graph [34, 56] or 2D top-down map [14, 35], modular-based methods benefit from the modularity and shorter time horizons. They are considered to be more sample efficient and generalizable [14, 35]. Recent progress in modular-based methods has proposed a frontier-based exploration strategy [35], a hallucinate-driven semantic mapping method [14], and novel verification stage [26]. In contrast with prior map-based works, our method utilizes 3D spatial knowledge, including 3D point semantic prediction and consistency, enabling a more comprehensive understanding of the environment.

**Embodied AI tasks with 3D Scene Representation.** There are considerable research leveraging 3D scene repre-

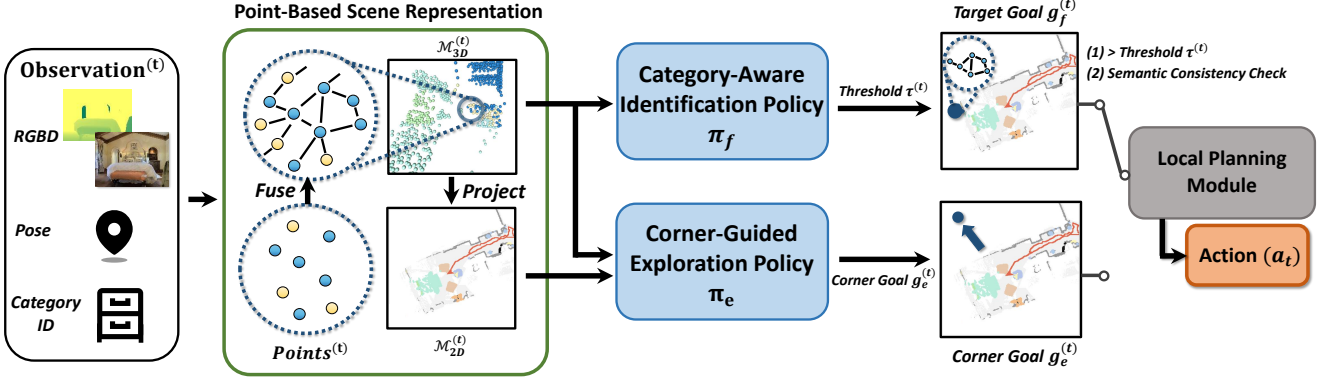


Figure 2. An overview of our framework. We take in a posed RGB-D image at time step  $t$  and perform point-based construction algorithm to online fuse a 3D scene representation ( $\mathcal{M}_{3D}^{(t)}$ ), along with a  $\mathcal{M}_{2D}^{(t)}$  from semantics projection. Then, we simultaneously leverage two policies, including a *corner-guided exploration policy*  $\pi_e$  and *category-aware identification policy*  $\pi_f$ , to predict a discrete corner goal  $g_e^{(t)}$  and a target goal  $g_f^{(t)}$  (if exist) respectively. Finally, the local planning module will drive the agent to the given target goal  $g_f^{(t)}$  (top priority) or the corner goal  $g_e^{(t)}$ .

sentation on certain embodied AI tasks, e.g., object grasping [5, 10], drawer opening [30, 44]. These works leverage various routes, including reinforcement learning [13], imitation learning [44], and supervised learning [5] with 3D scene representation, such as mesh, dense grids. However, most of these 3D-aware embodied AI tasks only perform in a limited space [10, 30, 44], e.g., near one table or drawer. Under large scale environments, such as floor-level scenes in ObjectNav, the existing methods would suffer from complex 3D observation and large computational costs. In this work, we propose a framework through leveraging a point-based construction module and two dedicatedly designed exploration and identification policies, to enable a 3D-aware agent for ObjectNav.

### 3. Method

#### 3.1. Task Definition and Method Overview

**Object Goal Navigation Task.** In an unknown environment, the Object Goal Navigation task requires the agent to navigate to an instance of the specified target category. For fair comparison, we follow the previous problem setting [38, 49]. As initialization, the agent is located randomly without access to a pre-built environment map, and provided with a target category ID. At each time step  $t$ , the agent receives noiseless onboard sensor readings, including an egocentric RGB-D image and a 3-DoF pose (2D position and 1D orientation) relative to the starting of the episode. Then the agent estimates its action  $a_t \in \mathcal{A}$  for movement in a discrete action space, consisting of `move_forward`, `turn_left`, `turn_right` and `stop`. Given a limited time budget of 500 steps, the agent terminates the movement until it is within 1 meter of an object of the specified category.

**Method Overview.** Figure 2 provides an overview of the proposed 3D-aware ObjectNav method. Our method takes RGBD frames along with pose sensor readings as input, to online construct a point-based scene representation  $\mathcal{M}_{3D}$  (Sec. 3.2), which is further projected to construct a 2D semantic map  $\mathcal{M}_{2D}$ . Given the structured 3D points  $\mathcal{M}_{3D}$  and 2D map  $\mathcal{M}_{2D}$ , our framework simultaneously performs two complementary policies (Sec. 3.3), the *exploration* policy and *identification* policy at a fixed time cycle of 25 steps. The exploration policy predicts a long-term discrete corner goal  $g_e$ , to drive the agent to explore the surrounding environment. Meanwhile, the identification policy evaluates the 3D points  $\mathcal{M}_{3D}$  at each step and outputs a target object goal  $g_f$  if its semantic prediction is confident and consistent. The  $g_f$  will be set as the approaching target for the agent once it exists, otherwise the agent will navigate to the long-term corner goal  $g_e$ . An underlying local planning module will navigate the agent towards the *goal* using analytical path planning.

#### 3.2. Navigation-Driven 3D Scene Construction

During navigation, the 3D-aware agent will constantly obtain new observations and incrementally build a fine-grained 3D scene representation, integrating spatial and semantic information to drive the agent. However, given that our agent is deployed for a floor-level GoalNav task, it is fairly challenging to construct and leverage 3D representation across the entire scene while keeping an acceptable computational cost. Accordingly in this section, we extend an online point-based construction algorithm [53] to online organize the 3D points and further empower semantic fusion and consistency estimation. This design is tailored for a comprehensive scene understanding of the ObjectNav agent, requiring little computational resources.

**3D Scene Representation.** At time step  $t$ , we represent the 3D scene  $\mathcal{M}_{3D}$  as the point clouds, denoted as  $P^{(t)} = \{(P_l^{(t)}, P_s^{(t)}, P_c^{(t)})\} \in \mathbb{R}^{N^{(t)} \times (M+4)}$ , where  $N^{(t)}$  is the point number. For each point  $i$ , the  $M + 4$  channels include the point position  $P_{i,l}^{(t)} \in \mathbb{R}^3$ , point semantics  $P_{i,s}^{(t)} \in \mathbb{R}^M$  and the point-wise spatial semantic consistency information  $P_{i,c}^{(t)} \in \mathbb{R}^1$ .

**Online 3D Point Fusion** Given a new captured posed RGB image  $I_c^{(t)}$  and depth image  $I_d^{(t)}$  at time step  $t$ , the agent can obtain the point position  $P_l^{(t)}$  by back-projecting all the depth images into the 3D world space via their corresponding poses. These points will be organized by a point-based construction algorithm [53]. Here, we briefly revisit this strategy.

The construction algorithm dynamically allocates occupied 3D blocks  $\{\mathcal{B}_k\}$  along with their index  $k$  maintained by a tree-based method [20]. Each block  $\mathcal{B}_k$  is defined by the boundary of constant length (10cm) along the X, Y and Z axes, e.g.,  $[X_{min}(\mathcal{B}_k), X_{max}(\mathcal{B}_k)]$ . And the points  $p_{l,x} \in [X_{min}(\mathcal{B}_k), X_{max}(\mathcal{B}_k)]$  (the same requirement holds for Y and Z axes) are recorded by the block  $\mathcal{B}_k$ . Given any 3D point  $p_i$ , the algorithm can achieve efficient neighborhood retrieval with the corresponding block index  $k$ . Furthermore, a one-level octree  $\mathcal{O}_i$  for each point  $p_i$  is constructed to obtain the fine-grained spatial information among points. Specifically, we connect each point with its nearest points in the eight quadrants of the Cartesian coordinate system (See Figure 3). Powered by this point-based construction strategy, give any point, we can efficiently query this point with its neighbor points by blocks retrieval and octree. This algorithm for organizing 3D points can run at 15 FPS while requiring reasonable memory resources (about  $\sim 500$  MB for one entire scene). We provide more detailed description in the the supplemental material.

**Online Semantic Fusion.** With an efficient reconstruction algorithm in hand, we can directly fuse temporal information, e.g., multi-view semantic predictions, to achieve more accurate and consistent scene understanding. Specifically, any point  $p_i$  which has been captured by a sequence of RGBD frames  $\{I_c^{(t)}, I_d^{(t)}\}$  could have multiple semantic predictions  $\{p_{i,s}^{(t)}(I_c^{(t)})\}$ . We thus propose to online aggregate the multi-view 2D semantic predictions using a max-fusion mechanism to obtain the final 3D semantic prediction:

$$p_{i,s}^{(t)} = \mathcal{N}(\max(\{p_{i,s}^{(t)}(I_c^{(t)})\})), \quad (1)$$

where the max is performed on each semantic category, followed by a normalization  $\mathcal{N}$  to linearly scale the probability distribution. Note that, the alternatives to fuse semantic predictions do exist, e.g. 3D convolution [19, 24], Bayesian updating [28]. However, directly conducting 3D convolution into such a floor-level 3D representation would in-

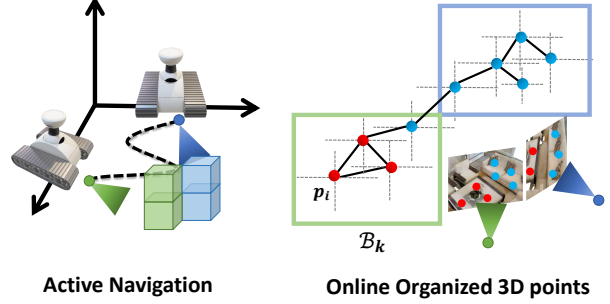


Figure 3. Illustration of online 3D point fusion. **(Left)** A robot takes multi-view observations during navigation. **(Right)** The points  $p$  are organized by dynamically allocated blocks  $\mathcal{B}$  and per-point octrees  $\mathcal{O}$ , which can be used to query neighborhood points of any given point.

evitably lead to a huge rise of computational cost, especially in the context of learning-based policy. We find that maximizing the 2D semantic prediction can already achieve impressive improvement on semantic accuracy (see Figure 8), with higher memory efficiency and time efficiency. Similar findings have also been reported and exploited in relevant works [7, 16].

**Spatial Semantic Consistency.** Based on the fact that semantic label should remain consistent for all the points in a single object, we propose to calculate the spatial semantic consistency information  $P_c^{(t)}$  as part of the navigation-driven 3D scene representation. To be specific,  $P_{i,c}^{(t)}$  is computed as the maximum semantic KL-divergence between point  $P_i^{(t)}$  and its octree  $\mathcal{O}(P_i^{(t)})$ :

$$P_{i,c}^{(t)} = \max(\{KL(P_{i,s}^{(t)}, P_{j,s}^{(t)}) | \forall P_j^{(t)} \in \mathcal{O}(P_i^{(t)})\}), \quad (2)$$

where  $KL$  denotes the KL-divergence computation, which is a statistical distance that measures the semantic probability distribution between  $P_{i,s}^{(t)}$  and  $P_{j,s}^{(t)}$ . Note for point  $P_i^{(t)}$ , if we count all its spatially close points as the neighbourhood  $\mathcal{N}(P_i^{(t)})$ , it could be time consuming to calculate Equation 2, and the spatially close points do not help relieve the issue of outlier points as mentioned above. Therefore, we use the pre-built octree  $\mathcal{O}_i$  to retrieve 8 nearest point in the quadrants of the Cartesian coordinate system.

### 3.3. Simultaneous Exploration and Identification

With the aggregated 3D information, we expect to empower a 3D-aware agent for the ObjectNav task. However, despite the efficient 3D scene representation, the agent still suffers from the complex and high-dimensional observations, leading to a lower sample efficiency in RL and hampering the navigation policy learning. Therefore, we leverage two complementary sub-policies: corner-guided exploration policy and category-aware identification policy. Each

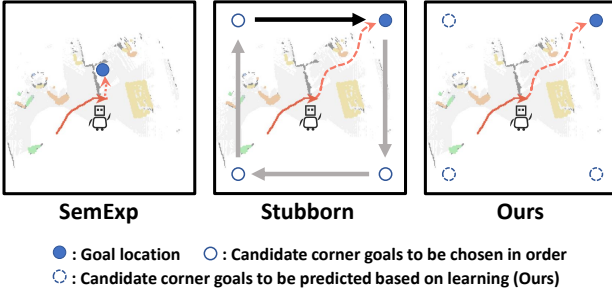


Figure 4. Illustration of exploration policy. (**Left**) Learning-based continuous global goal [9]; (**Middle**) Heuristic direction selection [26]; (**Right, ours**) Learning-based corner goal prediction.

policy learns to predict low-dimensional discrete actions and outputs a goal location to navigate the agent, resulting in a strong performance while requiring less training time. We will detail the two policies below.

**Observation Space.** At each time step  $t$ , both policies take fine-grained 3D observation  $x_{3D}^{(t)} = \{P^{(t)} \in ((4+m) \times N)\}$  based on 3D scene representation  $\mathcal{M}_{3D}$ . Here, the  $N$  indicates the point number (we sample 4096 points) and the  $m+4$  channels are comprised of point position  $p_l^{(t)} \in \mathbb{R}^3$ , fused semantic predictions  $p_s^{(t)} \in \mathbb{R}^m$  and spatial semantic consistency  $p_c^{(t)} \in \mathbb{R}^1$ . Following existing works [8, 9], we use an additional egocentric 2D map  $\mathcal{M}_{2D}$  for exploration policy and the local path planning module, which is directly obtained by a project-to-ground operation. More detailedly, for 2D observation  $x_{2D}^{(t)} \in ((2+m) \times M \times M)$  from 2D map  $\mathcal{M}_{2D}$ , the first two channels represent obstacles and explored area, and the rest of the channels each corresponds to an object category. Here,  $\mathcal{M}_{2D}$  (in a resolution of  $M = 240$  with 20cm grids) is constructed to give a large perception view of the scene, while 3D points perform as a fine-grained observation of objects. In addition to the scene representations, we also pass the goal object category index  $OID$  as the side input to both policies.

**Corner-Guided Exploration Policy.** The exploration policy attempts to guide the agent to explore and perceive the surrounding environment where it could access any instance of the target object category. We observe that existing learning-based exploration policies predict goal locations over the 2D map in continuous or large-dimensional discrete action space (Figure 4 Left), suffering from low sample efficiency. Therefore, we define a corner-guided exploration policy  $g_e = \pi_e(x_{3D}, x_{2D}, OID; \theta_e)$  that predicts a corner goal  $g_e$  to drive the agent (Figure 4 Right). Here, the  $\theta_e$  indicates the parameters of the policy, and  $g_e$  is one of the four pre-defined corner goals {Top Left, Top Right, Bottom Left, Bottom Right} of the 2D map.

Compared to predicting goals in a continuous or high-dimensional action space, learning to predict the four corner goals significantly reduces the learning difficulty. More-

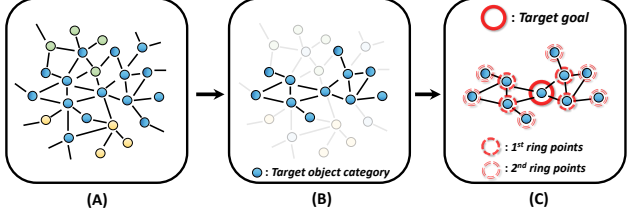


Figure 5. Illustration of identification policy. From A → B, fused points are filtered by the category-aware predicted threshold  $\tau$ . From B → C, the policy further checks the spatial label consistency of the points and identifies the target goal.

over, as noted by previous studies [4, 26], the corner-goal-based exploration strategy exhibits the capacity to achieve efficient exploration through avoiding back-and-forth pacing. Superior to using other heuristic corner goal exploration strategies (Figure 4 Middle), our agent can learn from the 3D scene priors to behave more intelligently. Demonstrations of our corner-guided exploration can be found in the attached video.

**Category-Aware Identification Policy.** During navigation, the agent consistently makes semantic predictions to identify an instance of target object category. Most works [9, 14] simply use a preset hard confidence threshold for target identification. However, this strategy is inherently sub-optimal due to the considerable variability in semantic prediction results across different categories and observation angles. As a result, a preset threshold would be unable to adequately adapt to the ever-changing nature of these scenarios. Also, it ignores to consider the consistency of the semantic prediction in 3D space.

To tackle this issue, we propose to leverage both dynamic confidence threshold and spatial semantic label consistency for target identification. We define a policy  $s = \pi_f(x_{3D}, OID; \theta_f)$  which takes the 3D observation  $x_{3D}$  and target category index  $OID$  and outputs a threshold-indicating action  $s \in \{0, 1, \dots, 9\}$ . And the dynamic threshold  $\tau$  can be obtained by:

$$\tau = \tau_{low} + s \cdot \frac{1 - \tau_{low}}{10}, \quad (3)$$

where the  $\tau_{low}$  is set to 0.5 in our implementation for a threshold range  $\tau \in [0.5, 0.95]$ . The  $\tau$  will be used to dynamically identify the points belonging to the target object (Figure 5 Middle). It is worth mentioning that this policy also utilizes a low-dimensional discrete action space, which is fairly easy for the agent to learn.

To obtain the final target goal  $g_f$ , our method further checks the spatial semantic label consistency. Specifically, we use the points  $\{p_i | (p_i, p) \in \mathcal{O}_p\}$  connected by the per-point octree  $\mathcal{O}_p$  to approximately represent the 3D surface of the target object. Our insight is that the points along the target's surface should have consistent semantic

labels. Therefore, we only identify those points who have at least 2-ring neighbors across the octrees  $\{p_i | (p_i, p_j) \in \mathcal{O}_{p_j} | (p_j, p) \in \mathcal{O}_p\}$  as the target object goal  $g_f$  (Figure 5 Right). See Figure 5 for visualized illustration and more details can be found in supplemental material.

**Local Planning Module.** The goals  $g_e$  and  $g_f$  from two policies will be consistently updated during navigation. Our method will preferentially utilize the target goal  $g_f$  if it exists, otherwise take the long-term corner goal  $g_e$  to explore. To navigate to the given location, we use the Fast Marching Method [42] to analytically plan the shortest path from the agent location. The agent then takes deterministic actions to follow this path.

**Rewards.** For the exploration policy, we share a similar reward design as [1, 51]. The agent receives a sparse success reward  $r_{success} = 2.5$ , a slack reward  $r_{slack} = 10^{-2}$  and an exploration reward  $r_{explore}$ . The exploration reward is a dense reward, defined by the number of new inserted point  $n_p^{new}$  as  $r_{explore} = n_p^{new} \times 10^{-3}$ . The slack reward and exploration reward encourage the agent to take the most effective direction to the unobserved area. And for the identification policy, we combine the same success reward and slack reward borrowed from the exploration policy.

## 4. Experiments

### 4.1. Experiment Setup.

We perform experiments on the Matterport3D (MP3D) [6] and Gibson [48] datasets with the Habitat simulator [39]. Both Gibson and MP3D contain photorealistic 3D reconstructions of real-world environments. For Gibson, we use 25 train / 5 val scenes from the Gibson tiny split. And we follow the same setting as in [9, 35] where we consider 6 goal categories, including *chair, couch, potted plant, bed, toilet* and *TV*. For MP3D, we use the standard split of 61 train / 11 val scenes with Habitat ObjectNav dataset [38], which consists of 21 goal categories (the full list can be found in the supplemental material). Note that, the RGB-D and pose readings are noise-free from simulation (follow the definition of [1]). Estimation of the pose from noisy sensor readings is out of the scope of this work and can be addressed if necessary, by incorporating off-the-shelf robust odometry [52, 54].

**Implementation Details.** On MP3D, we use the same pre-trained 2D semantic model RedNet [21] as [35, 51]. On Gibson, we leverage a Mask R-CNN [18], which is trained with COCO dataset [23]. For each frame, we randomly sample 512 points for point-based construction. Moreover, we use PointNet [33] and fully convolutional networks [25] to obtain the feature of 3D points and the 2D map, respectively. During training, we sample actions every 25 steps and use the Proximal Policy Optimization (PPO) [41] for both ex-

Table 1. ObjectNav validation results on Gibson and MP3D. Our method is trained with 5 seeds and report the averaged performance. The best of all methods and the best of all modular-based methods are highlighted in **bold** and underline colors, respectively. Note that Habitat-Web takes use of extra data.

Method	Gibson (val)			Matterport3D (val)		
	SPL(%)↑	Succ.(%)↑	DTS(m)↓	SPL(%)↑	Succ.(%)↑	DTS(m)↓
DD-PPO [47]	10.7	15.0	3.24	1.8	8.0	6.90
Red-Rabbit [51]	—	—	—	7.9	34.6	—
THAD [27]	—	—	—	11.1	28.4	5.58
Habitat-Web [36]	—	—	—	10.2	<b>35.4</b>	—
FBE [37]	28.3	64.3	1.78	7.2	22.7	6.70
ANS [8]	34.9	67.1	1.66	9.2	27.3	5.80
L2M* [14]	—	—	—	11.0	32.1	5.12
SemExp* [9]	39.6	71.7	1.39	10.9	28.3	6.06
Stubborn* [26]	—	—	—	13.5	31.2	5.01
PONI [35]	41.0	73.6	1.25	12.1	31.8	5.10
Ours	<b>42.1</b>	<u>74.5</u>	<u>1.16</u>	<u>14.6</u>	34.0	<b>4.74</b>

Table 2. ObjectNav validation results on MP3D-L2M [14].

Method	MP3D-L2M			
	SPL(%)↑	SoftSPL(%)↑	Succ.(%)↑	DTS(m)↓
SemExp [9]	16.5	—	28.1	4.848
L2M [14]	14.8	20.0	34.8	3.669
Ours	<b>21.2</b>	<b>30.5</b>	<b>40.2</b>	<b>3.278</b>

ploration and identification policies. More implementation details can be found in the supplemental material.

**Evaluation Metrics.** Following existing works [2, 14, 35], we adopt the following evaluation metrics: 1) SPL: success weighted by path length. It measures the efficiency of the agent over oracle path length, which serves as the primary evaluation metric for Habitat Challenge [49]. 2) Success rate: the percentage of successful episodes 3) Soft SPL: a softer version of SPL measure the progress towards the goal (even with 0 success). 4) DTS: geodesic distance (in m) to the success at the end of the episode.

**Baselines.** We consider mainstream baselines in the ObjectNav task. For end-to-end RL methods, we cover DD-PPO [47], Red-Rabbit [51], THDA [27], and Habitat-Web [36]. For modular based methods, we cover FBE [37], ANS [8], L2M [14], SemExp [9], Stubborn [26] and PONI [35]. Note that, some works use additional data to improve the performance, *e.g.* Habitat-web leverages human demonstration trajectories, and THDA utilizes data augmentation. It is challenging to compare all the methods fairly. Therefore, we are particularly interested in the three most relevant baselines: SemExp, Stubborn, and PONI. These three methods share the same 2D semantic predictors [18, 21] as our method.

## 4.2. Results

**Comparison on MP3D and Gibson.** We evaluate our approach on MP3D (val) and Gibson (val) with other baselines, including end-to-end RL(rows 1 - 4) and modular-

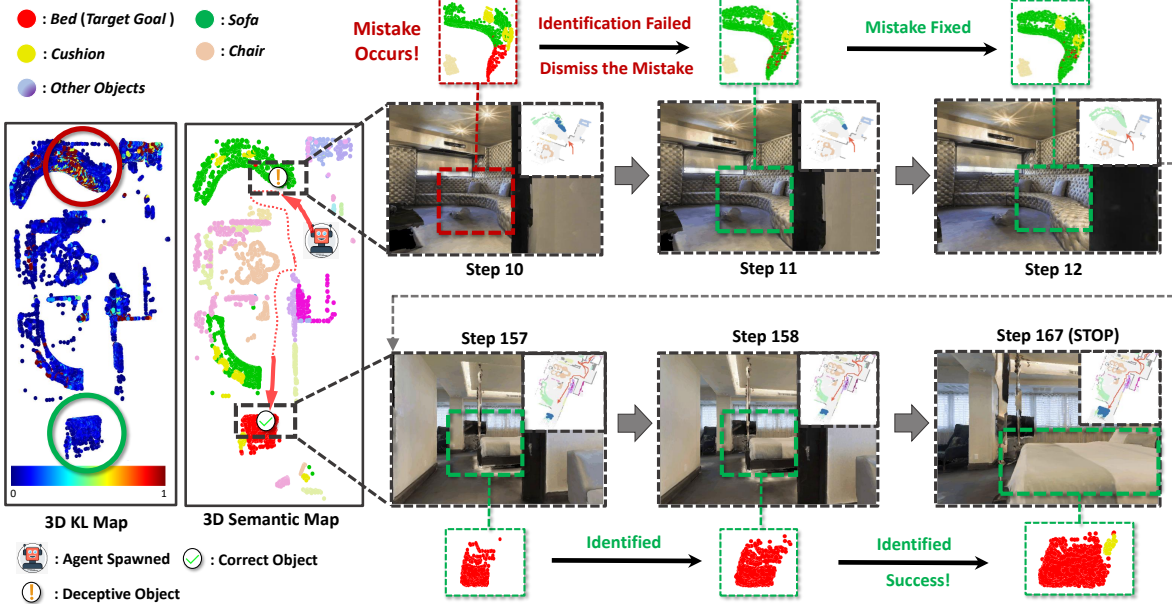


Figure 6. An qualitative visualization of the trajectory of the proposed method. We visualize an episode from MP3D where an agent is expected to find a *bed*. The semantic prediction  $p_s$  and spatial semantic consistency  $p_c$  of points are visualized on the left. During navigation, the agent can successfully dismiss the wrong prediction and approach and finally call stop around the target object.

Table 3. Comparison of different exploration policies. Here, all methods share the same identification strategy from [9] for fair comparison.

Method	SPL(%)	Succ.(%)	DTS(m)
Learn Continuous Goal.	11.1	28.6	6.354
Learn dense Grid Goal.	12.7	29.5	5.635
Learn 8 corner goal.	12.9	30.7	5.112
Heuristic. 4 corner goal.	13.5	33.0	4.995
Learn 4 corner goal. (Ours)	<b>13.9</b>	<b>33.5</b>	<b>4.931</b>

based methods(rows 5 - 10). Note that, SemExp and Stubborn did not report the results on MP3D validation, while L2M uses a self-made dataset MP3D-L2M based on MP3D and tests fewer categories than what we do. We therefore faithfully provide the results, denoted with \*, by evaluating with their public available code. The results are demonstrated in Table 1. On both datasets, our method achieves the state-of-the-art ObjctNav efficiency (SPL) among all methods (2.6% higher on Gibson dataset and 8.1% higher on MP3D). For the success rate, our method achieves the best results among all modular-based methods, showing comparable performance with additional annotation methods THAD [27] and Habitat-web [36]. Especially, compared with the modular-based methods, SemExp, Stubborn, and PONI, which share the same 2D semantic predictor [21] as ours, the results fairly demonstrate the superiority of our framework on both efficiency and success rate. We also provide the results validated on MP3D-L2M in Table 2.

We also provide a qualitative visualization of MP3D

Table 4. Comparison on different identification policies.

Method	Type	SPL(%)	Succ.(%)	DTS(m)
Deterministic	2D	0.85	12.8	30.1
	3D	0.85	13.8	32.5
Learning (Ours)	3D	-	<b>14.6</b>	<b>34.0</b>
				<b>4.749</b>

episodes in Figure 6. Here, our method online updates the semantic prediction and successfully dismisses the wrong target goal. For more qualitative results, please refer to the supplemental material.

**Comparison on Exploration Policy.** We conduct an experiment to verify the efficiency of our corner-guided exploration policy on MP3D. To remove the effect of the 2D semantic predictor and identification policy, all competitors share the same semantic predictor and a heuristic identification policy proposed in SemExp [9]. The results are reported in Table 3. Our corner-guided exploration policy outperforms the mainstream existing methods, including learning-based ones [8, 14] and heuristic ones [26]. Our findings indicate that the best performance is achieved through learning to predict discrete corner goals from the four corners of the scene. This suggests that the four-corner design, which benefits from a small, discrete action space, is already capable of efficiently guiding the agent in exploring the environment.

**Comparison on Identification Policy.** Another critical challenge in ObjctNav is how to properly identify an in-

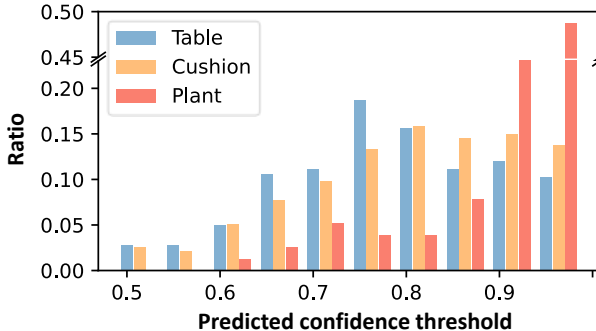


Figure 7. An comparison of predicted threshold distribution between different categories by our category-aware policy. We report the ratio of the each predicted threshold.

stance of target object category. Therefore, We evaluate our identification policy on MP3D along with other identifying strategies, including a 2D frame-based policy adopted in [9] and 3D point-based methods proposed by our approach. The results are shown in Table 4. We observe a performance improvement (rows 1 - 2) by simply leveraging 3D point-based construction and fusion algorithm. It can demonstrate that the multi-view observations provide more accurate semantic prediction, which effectively reduces false positive prediction (see examples in Figure 8). Moreover, our category-aware identification policy, through predicting dynamic threshold, demonstrates an even better performance.

To further investigate the effect of our identification policy, We conduct a break down study in Figure 7 by plotting the distribution of predicted semantic confidence thresholds. Specifically, we plot the distribution of three different categories (*table*, *cushion*, *plant*). For a relatively easy-to-recognize category, such as *table* with 52.6% success rate (SR), our policy predict a broad threshold distribution. However, for more challenging categories, such as *cushion* (36.9% SR) and *plant* (16.1% SR), the policy tends to be more conservative through setting a higher threshold. The results demonstrate the category-aware characteristic of our identification policy which adapts well to different difficulty levels across categories.

**Ablation Study.** We also perform an ablation study to verify the effectiveness of different components of our method. The results are demonstrated in Table 5. The cooperation of the 2D top-down map and 3D points (row 4) shows significant improvement by incorporating extensive scene perception (in 2D) and fine-grained object perception (in 3D). Moreover, rows (3-4) and (4-5) proved the effectiveness of leveraging consistency information and the identification policy, respectively.

**Analysis of Computational Cost.** Our framework is extremely memory efficient, which requires about 0.5GB for one scene, and can perform online construction and

Table 5. Ablation study of main components in our method. The pos. indicates the semantic predictions  $p_s$ , KL indicates the spatial semantic consistency  $p_c$  and the I. policy indicates the usage of the proposed identification policy.

2D map Pos.	3D points KL	I. Policy	SPL(%)	Succ.(%)	DTS(m)
✓			11.2	29.6	6.213
	✓	✓	13.0	32.3	5.769
✓	✓		13.7	33.8	5.620
✓	✓	✓	13.9	33.5	4.931
✓	✓	✓	14.6	34.0	4.749

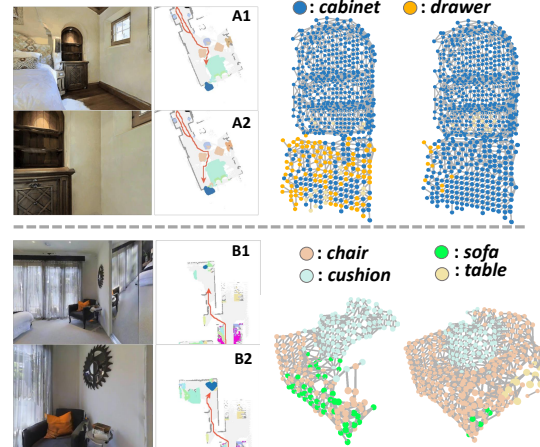


Figure 8. Visualization of the results of online 3D point fusion.

semantic fusion at a frame rate of 15 FPS. Moreover, our method requires only 48 GPU hours to train a 3D-aware agent on MP3D dataset to achieve the SOTA performance among all modular-based methods. This is significantly faster (30x) than other existing reinforcement learning based methods [9, 51], and is comparable to supervised learning modular-based methods [35].

## 5. Conclusion

In this work, we present a 3D-aware framework for object goal navigation. Our method is based on a 3D point-based construction algorithm to observe the 3D scenes and simultaneously perform exploration and identification policies to navigate the agent. Our method achieve SOTA performance among all modular-based methods, while requiring less training time. In the future, we would like to exploit this 3D-aware framework in other embodied AI tasks, e.g. mobile manipulation, robotic nurses.

**Acknowledgements.** We thank anonymous reviewers for their valuable suggestions. This work was supported by National Key Research and Development Program of China (2018AAA0102200), NSFC (62132021), and Beijing Academy of Artificial Intelligence (BAAI).

## References

- [1] Dhruv Batra, Aaron Gokaslan, Aniruddha Kembhavi, Oleksandr Maksymets, Roozbeh Mottaghi, Manolis Savva, Alexander Toshev, and Erik Wijmans. ObjectNav Revisited: On Evaluation of Embodied Agents Navigating to Objects. In *arXiv:2006.13171*, 2020. [2](#), [6](#), [13](#)
- [2] Dhruv Batra, Aaron Gokaslan, Aniruddha Kembhavi, Oleksandr Maksymets, Roozbeh Mottaghi, Manolis Savva, Alexander Toshev, and Erik Wijmans. Objectnav revisited: On evaluation of embodied agents navigating to objects. *ArXiv*, abs/2006.13171, 2020. [6](#)
- [3] Tommaso Campari, Paolo Eccher, Luciano Serafini, and Lamberto Ballan. Exploiting scene-specific features for object goal navigation. In *European Conference on Computer Vision*, pages 406–421. Springer, 2020. [1](#), [2](#)
- [4] Chao Cao, Hongbiao Zhu, Howie Choset, and Ji Zhang. Tare: A hierarchical framework for efficiently exploring complex 3d environments. In *Robotics: Science and Systems*, 2021. [5](#)
- [5] Hanwen Cao, Hao-Shu Fang, Wenhui Liu, and Cewu Lu. Suctionnet-1billion: A large-scale benchmark for suction grasping. *IEEE Robotics and Automation Letters*, 6(4):8718–8725, 2021. [3](#)
- [6] Angel Chang, Angela Dai, Thomas Funkhouser, Maciej Halber, Matthias Niessner, Manolis Savva, Shuran Song, Andy Zeng, and Yinda Zhang. Matterport3d: Learning from rgb-d data in indoor environments. *arXiv preprint arXiv:1709.06158*, 2017. [6](#), [13](#)
- [7] Devendra Singh Chaplot, Murtaza Dalal, Saurabh Gupta, Jitendra Malik, and Russ R Salakhutdinov. Seal: Self-supervised embodied active learning using exploration and 3d consistency. *Advances in Neural Information Processing Systems*, 34:13086–13098, 2021. [2](#), [4](#)
- [8] Devendra Singh Chaplot, Dhiraj Gandhi, Saurabh Gupta, Abhinav Gupta, and Ruslan Salakhutdinov. Learning to explore using active neural slam. *arXiv preprint arXiv:2004.05155*, 2020. [1](#), [2](#), [5](#), [6](#), [7](#), [13](#)
- [9] Devendra Singh Chaplot, Dhiraj Prakashchand Gandhi, Abhinav Gupta, and Russ R Salakhutdinov. Object goal navigation using goal-oriented semantic exploration. *Advances in Neural Information Processing Systems*, 33:4247–4258, 2020. [1](#), [2](#), [5](#), [6](#), [7](#), [8](#), [13](#)
- [10] Changhyun Choi, Wilko Schwarting, Joseph DelPreto, and Daniela Rus. Learning object grasping for soft robot hands. *IEEE Robotics and Automation Letters*, 3(3):2370–2377, 2018. [3](#)
- [11] Sungjoon Choi, Qian-Yi Zhou, and Vladlen Koltun. Robust reconstruction of indoor scenes. In *Proceedings of the IEEE Conference on Computer Vision and Pattern Recognition*, pages 5556–5565, 2015. [14](#)
- [12] Angela Dai and Matthias Nießner. 3dmv: Joint 3d-multi-view prediction for 3d semantic scene segmentation. In *ECCV*, 2018. [1](#)
- [13] Samir Yitzhak Gadre, Kiana Ehsani, and Shuran Song. Act the part: Learning interaction strategies for articulated object part discovery. *ICCV*, 2021. [3](#)
- [14] Georgios Georgakis, Bernadette Bucher, Karl Schmeckepfer, Siddharth Singh, and Kostas Daniilidis. Learning to map for active semantic goal navigation. In *International Conference on Learning Representations (ICLR)*, 2022. [1](#), [2](#), [5](#), [6](#), [7](#), [13](#)
- [15] Georgios Georgakis, Yimeng Li, and Jana Kosecka. Simultaneous mapping and target driven navigation. *ArXiv*, abs/1911.07980, 2019. [2](#)
- [16] Margarita Grinvald, Fadri Furrer, Tonci Novkovic, Jen Jen Chung, Cesar Cadena, Roland Siegwart, and Juan Nieto. Volumetric instance-aware semantic mapping and 3d object discovery. *IEEE Robotics and Automation Letters*, 4(3):3037–3044, 2019. [4](#)
- [17] Saurabh Gupta, Varun Tolani, James Davidson, Sergey Levine, Rahul Sukthankar, and Jitendra Malik. Cognitive mapping and planning for visual navigation. *International Journal of Computer Vision*, 128:1311–1330, 2017. [2](#)
- [18] Kaiming He, Georgia Gkioxari, Piotr Dollár, and Ross B. Girshick. Mask r-cnn. *IEEE Transactions on Pattern Analysis and Machine Intelligence*, 42:386–397, 2020. [6](#)
- [19] Shi-Sheng Huang, Ze-Yu Ma, Tai-Jiang Mu, Hongbo Fu, and Shi-Min Hu. Supervoxel convolution for online 3d semantic segmentation. *ACM Transactions on Graphics (TOG)*, 40(3):1–15, 2021. [4](#)
- [20] Hosagrahar V Jagadish, Beng Chin Ooi, Kian-Lee Tan, Cui Yu, and Rui Zhang. idistance: An adaptive b+-tree based indexing method for nearest neighbor search. *ACM Transactions on Database Systems (TODS)*, 30(2):364–397, 2005. [4](#)
- [21] Jindong Jiang, Lunan Zheng, Fei Luo, and Zhijun Zhang. Rednet: Residual encoder-decoder network for indoor rgb-d semantic segmentation. *arXiv preprint arXiv:1806.01054*, 2018. [6](#), [7](#)
- [22] Cheng Lin, Tingxiang Fan, Wenping Wang, and Matthias Nießner. Modeling 3d shapes by reinforcement learning. In *ECCV*, 2020. [2](#)
- [23] Tsung-Yi Lin, Michael Maire, Serge J. Belongie, James Hays, Pietro Perona, Deva Ramanan, Piotr Dollár, and C. Lawrence Zitnick. Microsoft coco: Common objects in context. In *ECCV*, 2014. [6](#)
- [24] Leyao Liu, Tian Zheng, Yun-Jou Lin, Kai Ni, and Lu Fang. Ins-conv: Incremental sparse convolution for online 3d segmentation. In *Proceedings of the IEEE/CVF Conference on Computer Vision and Pattern Recognition*, pages 18975–18984, 2022. [4](#)
- [25] Jonathan Long, Evan Shelhamer, and Trevor Darrell. Fully convolutional networks for semantic segmentation. In *Proceedings of the IEEE conference on computer vision and pattern recognition*, pages 3431–3440, 2015. [6](#), [13](#)
- [26] Haokuan Luo, Albert Yue, Zhang-Wei Hong, and Pulkit Agrawal. Stubborn: A strong baseline for indoor object navigation. *arXiv preprint arXiv:2203.07359*, 2022. [2](#), [5](#), [6](#), [7](#), [13](#)
- [27] Oleksandr Maksymets, Vincent Cartillier, Aaron Gokaslan, Erik Wijmans, Wojciech Galuba, Stefan Lee, and Dhruv Batra. Thda: Treasure hunt data augmentation for semantic navigation. In *Proceedings of the IEEE/CVF International*

- Conference on Computer Vision*, pages 15374–15383, 2021. [1](#), [2](#), [6](#), [7](#)
- [28] John McCormac, Ankur Handa, Andrew Davison, and Stefan Leutenegger. Semanticfusion: Dense 3d semantic mapping with convolutional neural networks. In *2017 IEEE International Conference on Robotics and automation (ICRA)*, pages 4628–4635. IEEE, 2017. [4](#)
- [29] Arsalan Mousavian, Alexander Toshev, Marek Fišer, Jana Košecká, Ayzaan Wahid, and James Davidson. Visual representations for semantic target driven navigation. In *2019 International Conference on Robotics and Automation (ICRA)*, pages 8846–8852. IEEE, 2019. [2](#)
- [30] Tongzhou Mu, Zhan Ling, Fanbo Xiang, Derek Cathera Yang, Xuanlin Li, Stone Tao, Zhiao Huang, Zhiwei Jia, and Hao Su. Maniskill: Generalizable manipulation skill benchmark with large-scale demonstrations. In *Thirty-fifth Conference on Neural Information Processing Systems Datasets and Benchmarks Track (Round 2)*, 2021. [3](#)
- [31] Alexey Nekrasov, Jonas Schult, Or Litany, B. Leibe, and Francis Engelmann. Mix3d: Out-of-context data augmentation for 3d scenes. *2021 International Conference on 3D Vision (3DV)*, pages 116–125, 2021. [1](#)
- [32] Emilio Parisotto and Ruslan Salakhutdinov. Neural map: Structured memory for deep reinforcement learning. *ArXiv*, abs/1702.08360, 2018. [2](#)
- [33] C. Qi, Hao Su, Kaichun Mo, and Leonidas J. Guibas. Pointnet: Deep learning on point sets for 3d classification and segmentation. *2017 IEEE Conference on Computer Vision and Pattern Recognition (CVPR)*, pages 77–85, 2017. [6](#), [13](#)
- [34] Yiding Qiu, Anwesan Pal, and Henrik I Christensen. Learning hierarchical relationships for object-goal navigation. *arXiv preprint arXiv:2003.06749*, 2020. [1](#), [2](#)
- [35] Santhosh Kumar Ramakrishnan, Devendra Singh Chaplot, Ziad Al-Halah, Jitendra Malik, and Kristen Grauman. Poni: Potential functions for objectgoal navigation with interaction-free learning. In *Proceedings of the IEEE/CVF Conference on Computer Vision and Pattern Recognition*, pages 18890–18900, 2022. [1](#), [2](#), [6](#), [8](#)
- [36] Ram Ramrakhyा, Eric Undersander, Dhruv Batra, and Abhishek Das. Habitat-web: Learning embodied object-search strategies from human demonstrations at scale. In *Proceedings of the IEEE/CVF Conference on Computer Vision and Pattern Recognition*, pages 5173–5183, 2022. [1](#), [6](#), [7](#)
- [37] Ieee Robotics. Proceedings 1997 ieee international symposium on computational intelligence in robotics and automation circa'97 - towards new computational principles for robotics and automation, july 10-11, 1997, monterey, california, usa. In *CIRA*, 1997. [6](#)
- [38] Manolis Savva, Abhishek Kadian, Oleksandr Maksymets, Yili Zhao, Erik Wijmans, Bhavana Jain, Julian Straub, Jia Liu, Vladlen Koltun, Jitendra Malik, et al. Habitat: A platform for embodied ai research. In *Proceedings of the IEEE/CVF International Conference on Computer Vision*, pages 9339–9347, 2019. [1](#), [3](#), [6](#), [14](#)
- [39] Manolis Savva, Abhishek Kadian, Oleksandr Maksymets, Yili Zhao, Erik Wijmans, Bhavana Jain, Julian Straub, Jia Liu, Vladlen Koltun, Jitendra Malik, Devi Parikh, and Dhruv Batra. Habitat: A Platform for Embodied AI Research. In *Proceedings of the IEEE/CVF International Conference on Computer Vision (ICCV)*, 2019. [6](#)
- [40] Thomas Schops, Torsten Sattler, and Marc Pollefeys. Bad slam: Bundle adjusted direct rgb-d slam. In *Proceedings of the IEEE/CVF Conference on Computer Vision and Pattern Recognition*, pages 134–144, 2019. [2](#)
- [41] John Schulman, Filip Wolski, Prafulla Dhariwal, Alec Radford, and Oleg Klimov. Proximal policy optimization algorithms. *ArXiv*, abs/1707.06347, 2017. [6](#)
- [42] James A. Sethian. Fast marching methods. *SIAM Rev.*, 41:199–235, 1999. [6](#)
- [43] Nur Muhammad Mahi Shafullah, Chris Paxton, Lerrel Pinto, Soumik Chintala, and Arthur Szlam. Clip-fields: Weakly supervised semantic fields for robotic memory. *arXiv preprint arXiv:2210.05663*, 2022. [1](#)
- [44] Hao Shen, Weikang Wan, and He Wang. Learning category-level generalizable object manipulation policy via generative adversarial self-imitation learning from demonstrations. *arXiv preprint arXiv:2203.02107*, 2022. [3](#)
- [45] Thang Vu, Kookhoi Kim, Tung Minh Luu, Xuan Thanh Nguyen, and Chang-Dong Yoo. Softgroup for 3d instance segmentation on point clouds. *ArXiv*, abs/2203.01509, 2022. [1](#)
- [46] Thomas Whelan, Stefan Leutenegger, Renato Salas-Moreno, Ben Glocker, and Andrew Davison. Elasticfusion: Dense slam without a pose graph. *Robotics: Science and Systems*, 2015. [2](#)
- [47] Erik Wijmans, Abhishek Kadian, Ari Morcos, Stefan Lee, Irfan Essa, Devi Parikh, Manolis Savva, and Dhruv Batra. Dd-ppo: Learning near-perfect pointgoal navigators from 2.5 billion frames. *arXiv preprint arXiv:1911.00357*, 2019. [1](#), [2](#), [6](#)
- [48] Fei Xia, Amir R Zamir, Zhiyang He, Alexander Sax, Jitendra Malik, and Silvio Savarese. Gibson env: Real-world perception for embodied agents. In *Proceedings of the IEEE conference on computer vision and pattern recognition*, pages 9068–9079, 2018. [6](#)
- [49] Karmesh Yadav, Santhosh Kumar Ramakrishnan, John Turner, Aaron Gokaslan, Oleksandr Maksymets, Rishabh Jain, Ram Ramrakhyā, Angel X Chang, Alexander Clegg, Manolis Savva, Eric Undersander, Devendra Singh Chaplot, and Dhruv Batra. Habitat challenge 2022. <https://aihabitat.org/challenge/2022/>, 2022. [1](#), [2](#), [3](#), [6](#)
- [50] Wei Yang, Xiaolong Wang, Ali Farhadi, Abhinav Gupta, and Roozbeh Mottaghi. Visual semantic navigation using scene priors. *arXiv preprint arXiv:1810.06543*, 2018. [2](#)
- [51] Joel Ye, Dhruv Batra, Abhishek Das, and Erik Wijmans. Auxiliary tasks and exploration enable objectgoal navigation. In *Proceedings of the IEEE/CVF International Conference on Computer Vision*, pages 16117–16126, 2021. [1](#), [2](#), [6](#), [8](#)
- [52] Jiazhao Zhang, Yijie Tang, He Wang, and Kai Xu. Asradio: Active subspace random optimization based depth inertial odometry. *IEEE Transactions on Robotics*, 2022. [6](#)
- [53] Jiazhao Zhang, Chenyang Zhu, Lintao Zheng, and Kai Xu. Fusion-aware point convolution for online semantic 3d scene

- segmentation. In *Proceedings of the IEEE/CVF Conference on Computer Vision and Pattern Recognition*, pages 4534–4543, 2020. [2](#), [3](#), [4](#), [12](#)
- [54] Xiaoming Zhao, Harsh Agrawal, Dhruv Batra, and Alexander G. Schwing. The surprising effectiveness of visual odometry techniques for embodied pointgoal navigation. *2021 IEEE/CVF International Conference on Computer Vision (ICCV)*, pages 16107–16116, 2021. [6](#)
- [55] Lintao Zheng, Chenyang Zhu, Jiazhao Zhang, Hang Zhao, Hui Huang, Matthias Nießner, and Kai Xu. Active scene understanding via online semantic reconstruction. *Computer Graphics Forum*, 38, 2019. [2](#)
- [56] Fengda Zhu, Xiwen Liang, Yi Zhu, Qizhi Yu, Xiaojun Chang, and Xiaodan Liang. Soon: Scenario oriented object navigation with graph-based exploration. In *Proceedings of the IEEE/CVF Conference on Computer Vision and Pattern Recognition*, pages 12689–12699, 2021. [1](#), [2](#)
- [57] Yuke Zhu, Roozbeh Mottaghi, Eric Kolve, Joseph J. Lim, Abhinav Kumar Gupta, Li Fei-Fei, and Ali Farhadi. Target-driven visual navigation in indoor scenes using deep reinforcement learning. *2017 IEEE International Conference on Robotics and Automation (ICRA)*, pages 3357–3364, 2017. [2](#)

# Appendix

We provide additional information about our method, experiment settings and supporting qualitative visualizations. Below is a summary of the sections in the supplementary:

- Section A reports the details of 3D points construction algorithm.
- Section B reports the details of simultaneously running exploration and identification policies.
- Section C reports the computational cost of the proposed method.
- Section D reports the details of datasets used in our experiments.
- Section E reports additional experiments.
- Section F shows detailed progressive results of the proposed method on Matterport3D.

## A. 3D Point Fusion Implementation Details

We introduce the 3D point construction algorithm [53] utilized in our paper (Figure 9). The inputs of the construction algorithm are a sequence of posed color image  $I_c^{(t)}$  and depth images  $I_d^{(t)}$  at time step  $t$ . First, we can obtain the 3D points  $p$  via back-projection. Then, we dynamically allocate 3D blocks  $\{\mathcal{B}_k\}$ , which are composed of the occupied 3D points. To be specific, we divide the 3D world space into a set of adjacent 3D blocks  $\{\mathcal{B}_k\}$ , where each block  $B_k$  is defined by the boundary of constant length  $\tau_b$  along the X, Y and Z axes, e.g.,  $[X_{min}(B_k), X_{max}(B_k)]$ . Two adjacent blocks  $B_k, B_j$  along the X axis meet the requirement,  $X_{min}(B_k) = X_{max}(B_j)$  or  $X_{max}(B_k) = X_{min}(B_j)$ . The same requirement holds for Y and Z axes. Given the scene point cloud  $P^{(t-1)}$  at time step  $t-1$ , we allocate all the 3D points into each of the 3D blocks  $\{\mathcal{B}_k\}$ , hence a block-wise point retrieval can be easily achieved.

After constructing the blocks, we can achieve efficient point searching and neighborhood retrieval for any given 3D point  $p$ . However, the points within blocks are still unstructured. To obtain the fine-grained relationship of points, we further build a one-level octree  $\mathcal{O}_i$  for each point  $p_i \in P$ . Specifically, for each 3D point back-projected from the instant sensor reading, we perform its nearest neighbor search only among its occupied 3D block and adjacent blocks. Then, we connect the point with the nearest points in the eight quadrants of the Cartesian coordinate system. Now, given any point, we can search the nearest points in eight directions and expand the search region as large as we want. In our implementation, we randomly sample 512 points for

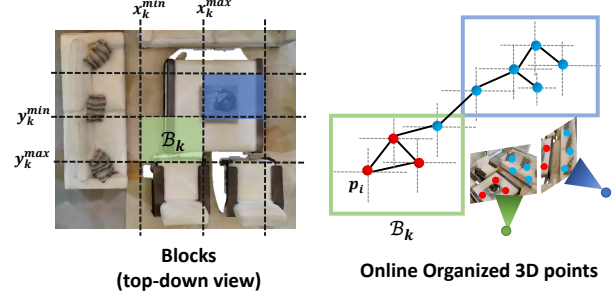


Figure 9. Illustration of online 3D point fusion. **(Left)** dynamically allocated blocks  $\mathcal{B}$  based on coordinate intervals . **(Right)** The points  $p$  are organized by blocks  $\mathcal{B}$  and per-point octrees  $\mathcal{O}$ , which can be used to query neighborhood points of any given point.

---

### Algorithm 1: Simultaneous Exploration and Identification for 3D-Aware ObjectNav

---

```

Input : Existed reconstructed points  $P_{l,s,c}^{(ts)}$ , RGB image  $I_c^{(t)}$ , Depth image  $I_d^{(t)}$ , Agent Pose  $o_{pose}^{(t)}$ , Target category index  $OID$  at time step  $t$ .
Output: Agent action  $a^{(t)}$ .
// Output a low-level action to drive the agent
//  $a^{(t)} \in \{\text{move\_forward}, \text{turn\_left}, \text{turn\_right} \text{ and } \text{stop}\}$ 
1  $P_{l,s}^{(t)} \leftarrow \text{BackProject}(I_d^{(t)}, \text{SemanticPredictor}(I_c^{(t)}))$ ;
// Obtain the location and semantic prediction of observed points
2  $P_{l,s}^{(ts)} \leftarrow \text{PointFusion}(P_{l,s}^{(ts)}, P_{l,s}^{(t)})$ ;
3  $P_c^{(ts)} \leftarrow \text{UpdateConsistency}(P_{l,s}^{(ts)})$ ;
// Fuse the new captured points and update the consistency
4  $g_e^{(t)} \leftarrow \text{ExplorationPolicy}(P_{l,s,c}^{(ts)}, \text{Project}(P_{l,s,c}^{(ts)}))$ ;
5  $\tau^{(t)} \leftarrow \text{IdentificationPolicy}(P_{l,s,c}^{(ts)})$ ;
6 if  $p \in P_{l,s,c}$  satisfy  $p_s > \tau^{(t)}$  and  $\text{ConsistencyCheck}(p, OID, P_{l,s,c})$  then
7    $g_f^{(t)} \leftarrow \text{Location}(p)$ ;
// Simultaneously run the exploration and identification policies
8 if  $g_f^{(t)}$  exists then
9    $a^{(t)} \leftarrow \text{Planning}(g_f^{(t)})$ ;
10 else
11    $a^{(t)} \leftarrow \text{Planning}(g_e^{(t)})$ ;
12 return  $a^{(t)}$ ;

```

---

each frame. And we only connect the points with distance range in [4cm, 15cm].

## B. Pipeline Implementation Details

In Algorithm 1, we describe the the details of simultaneously running exploration and identification policies. Here, we reuse the notions in the main paper.

### B.1. Policy Implementation Details

Our **corner-guided exploration policy** takes the 3D observation  $x_3D^{(t)}$ , 2D observation  $x_2D^{(t)}$  and extra information as inputs. The extra information comprises the

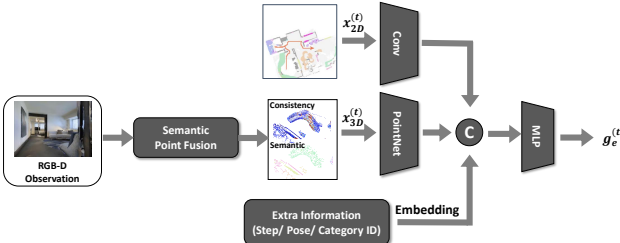


Figure 10. Network architecture of our exploration policy

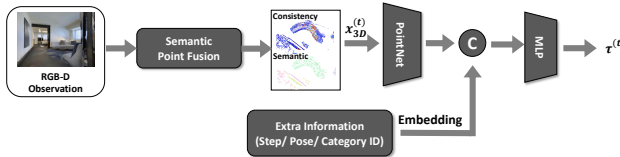


Figure 11. Network architecture of our verification policy

agent’s pose, the number of steps, and the target category ID. The proposed exploration policy predicts a discrete corner goal  $g_e^{(t)}$  to navigate the robot (Figure 10). Specifically, the policy uses a PointNet [33] to encode the 3D points information (position  $p_l^{(t)}$ , semantics  $p_s^{(t)}$ , and consistency  $p_c^{(t)}$ ) to obtain a global feature (256D). The 2D top-down map will be passed to a fully convolutional network [25] and flattened to a feature vector (256D). And the extra information is embedded into a feature vector (24D). Note that the processing of the 2D top-down map and extra information has also been reported in other existing methods [8, 9]. Then, the three feature vectors are concatenated and sent to linear networks, which will output the final target corner goal  $g_e^{(t)}$ . The **category-aware identification policy** takes 3D observation  $x_{3D}^{(t)}$  and extra information as inputs, and uses the same 3D observation and extra information branches as exploration policy. The identification policy outputs the threshold  $\tau^{(t)}$  for target goal selection (See algorithm 1).

## C. Computational Cost

Due to the fact that there are always significant overlaps between consecutive frames, when we perform point fusion, we can reuse most of the constructed 3D blocks ( $\sim 60\%$ ). Our algorithm for constructing the 3D scene representation runs at 15 FPS. The memory requirement of one scene can range from 200MB to 500MB during navigation.

We have implemented our core algorithm in python, PyTorch and PyCUDA. Both the point construction and policies run on a workstation with an Intel® Xeon® Gold 6240 CPU @ 3.50GHz  $\times$  12 with 64GB RAM and an Nvidia V100 GPU with 32GB memory.

Method	SPL(%)	Improvement
(1.a) 4 corner goal heuristics w/o iden. policy	13.1	-
(1.b) 4 corner goal heuristics w/ iden. policy	13.9	6.1% $\uparrow$
(2.a) learn continuous goal policy w/o iden. policy	10.1	-
(2.b) learn continuous goal policy w/ iden. policy	12.7	25.7% $\uparrow$
<b>(Ours)</b> learn 4 corner goal w/o iden. policy	13.7	-
<b>(Ours)</b> learn 4 corner goal w/ iden. policy	14.6	6.6% $\uparrow$

Table 6. More ablations on exploration and identification policies.

Noise Setting	SPL (%)	Succ. (%)	DTS (m)
(1) Ours (noiseless)	14.6	34.0	4.74
(2) w. Noisy Pose	13.5	33.1	5.51
(3) w. Gau. Noisy Depth	14.3	33.6	5.36
(4) w. Rdw. Noisy Depth	13.7	31.7	5.45
(5) w. Noisy Depth (Gau.) and Noisy Pose	13.6	31.6	5.50
(6) w. Noisy Depth (Rdw.) and Noisy Pose	13.1	30.1	6.02
(7) PONI (baseline, noiseless)	12.1	31.8	5.10
(8) Stubborn (baseline, noiseless)	13.5	31.2	5.01

Table 7. Results under various noise settings. Gau. indicates Gaussian. Rdw. indicates Redwood.

## D. Dataset

Here, we provide further details of the datasets where we validate our method for reference.

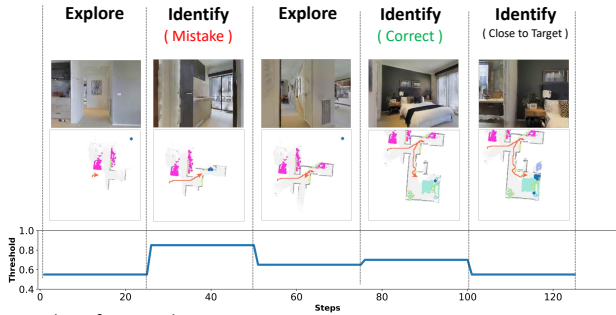
**Matterport 3D (MP3D)** [6] MP3D offers photorealistic reconstructions of building-scale scenes. Following the setting in Habitat Challenge 2021 [1], we consider 21 object categories: *chair*, *table*, *picture*, *cabinet*, *cushion*, *sofa*, *bed*, *chest of drawers*, *plant*, *sink*, *toilet*, *stool*, *towel*, *tv monitor*, *shower*, *bathtub*, *counter*, *fireplace*, *gym equipment*, *seating* and *clothes*. We split the dataset into 61 train / 11 val scenes, containing 2,632,422 / 2,195 episodes, respectively.

**MP3D-L2M.** In L2M [14], they validate their method on a self-made dataset consisting of 781 episodes from 10 MP3D (val) scenes, which we call MP3D-L2M. It covers 6 object categories: *chair*, *couch(sofa)*, *plant*, *bed*, *toilet* and *tv*. For a fair comparison, we also report our validation results on this MP3D-L2M in main paper table 2.

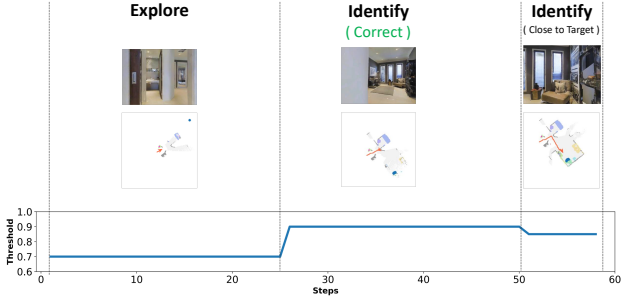
## E. Additional Experiments

**Ablation study on exploration and identification policies.** As shown in Table 6, 1) coupling our identification policy with exploration heuristics [26]; 2) joint learning our policy with 2D map-based exploration policy [9] till **full convergence** using double training steps of [9]. We observe that the results of various methods are improved by our identification policy, especially the continuous goal exploration strategy (25.7%  $\uparrow$  on SPL). Moreover, the fully trained continuous goal strategy does not outperform our corner-guided method, due to larger action space and therefore a harder RL problem.

#### A. Looking for a *chest of drawers*:



#### B. Looking for a *cushion*:



#### C. Looking for a *counter*:

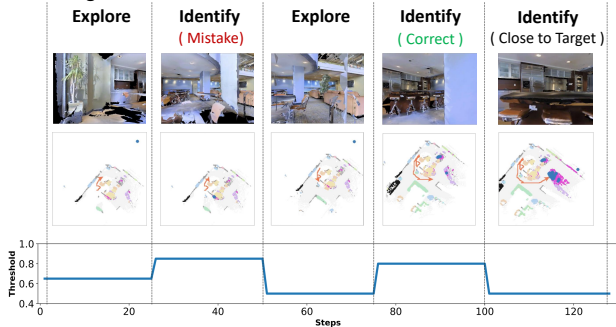


Figure 12. Visualization of threshold changes during navigation.

**Robustness to noises.** We conduct a series of experiments (Table 7) to evaluate our method with noisy pose and various depth noise models. Specifically, for the pose noise, we adopt the same simulation methods as in [38]; for depth noise, we consider Redwood [11] noise model and Gaussian noise model. Under the most challenging noises setting (6), our method has a minor drop of 1.5 point on SPL, which however still performs as a strong competitor against the noiseless baselines (7, 8).

**Qualitative examples of the identification policy.** Here we provide three qualitative examples (Figure 12) of our identification policy to navigate to various target objects. Note that, the identification policy is executed every 25 steps for the purpose of acceleration. Accordingly, we delineate the exploration and identification phases based on the primary policy utilized during the 25-step interval.

Based on the experimental results, the predicted thresh-

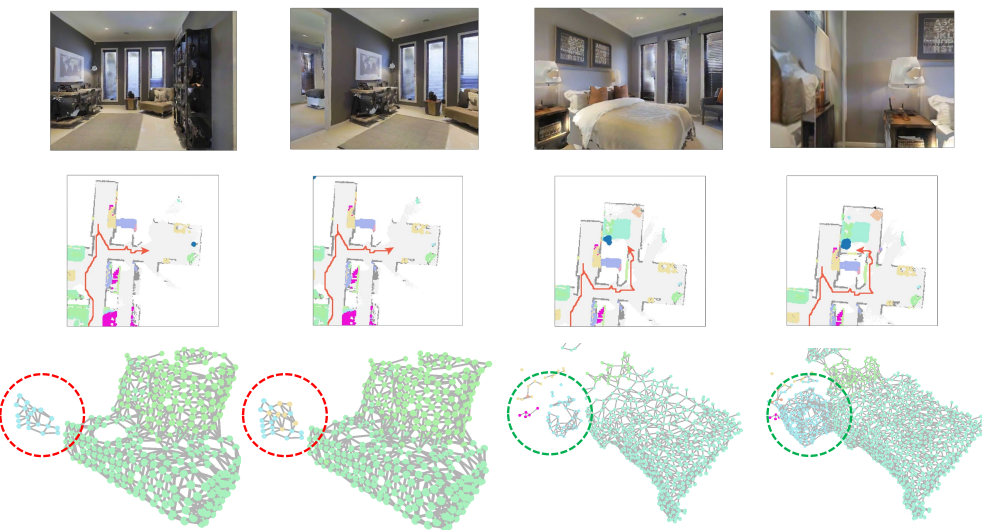
old is dynamically adjusted during navigation. Specifically, when the agent is under the control of the exploration policy, the identification policy predicts a relatively low threshold to facilitate rapid searching of potential targets. Conversely, when the agent is guided by the identification policy, the threshold is fine-tuned to achieve a trade-off between accuracy and efficiency. In general, the identification policy gives a high threshold to ensure a successful stop. Nevertheless, in the event that the agent is in close proximity to the target object, a low threshold is predicted for a quick stop.

## F. Visualizing ObjectNav episodes

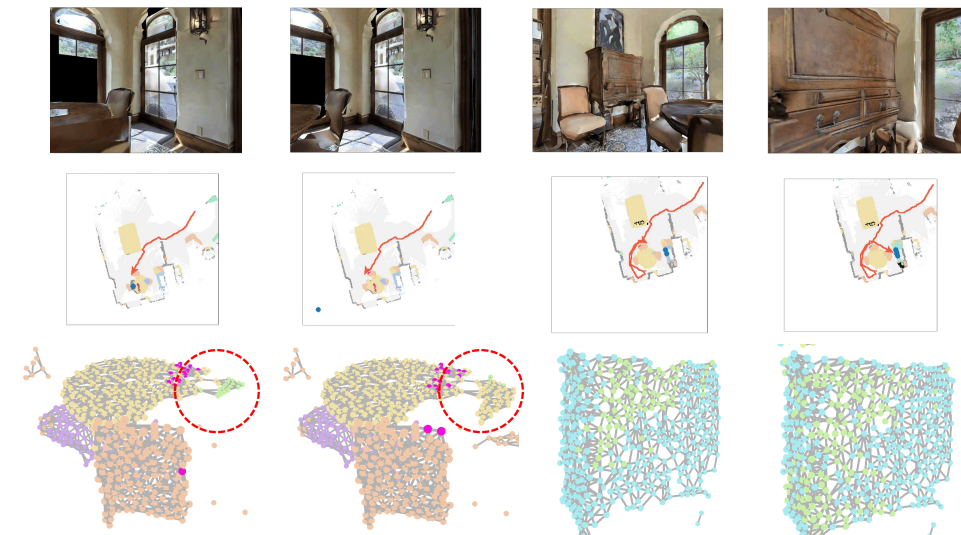
Figure 13 and Figure 14 illustrate a more detailed visualization of the results obtained through the implementation of our 3D point-based fusion algorithm on the Matterport3D Dataset. It can be observed that during navigation, there is a significant improvement in the semantic prediction and spatial consistency of the points. To further substantiate these findings, Figure 15 to 17 provide visualizations of additional episodes. For a comprehensive demonstration, the attached video in the supplemental material is recommended.



episode of finding a *drawer*



episode of finding a *cabinet*



episode of finding a *cushion*

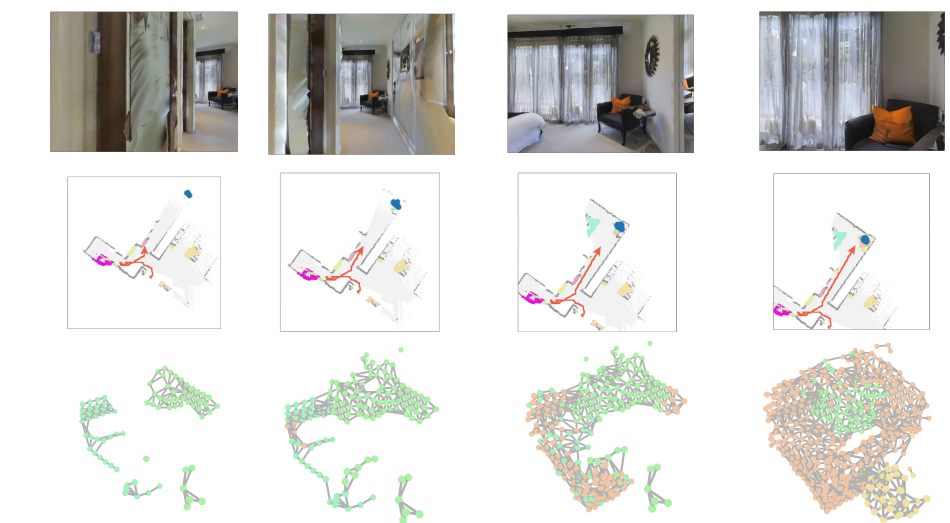
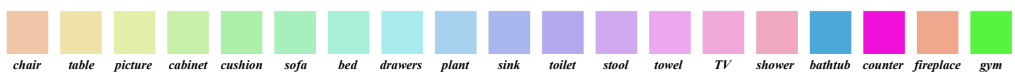


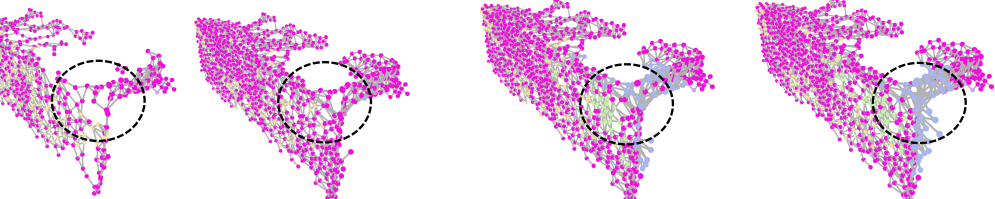
Figure 13. EPS Page1.



**episode of finding a chair**



**episode of finding a sink**



**episode of finding a table**

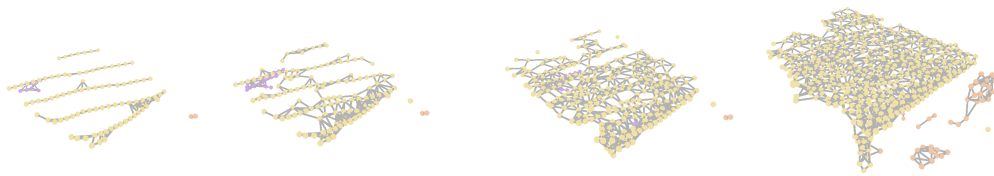
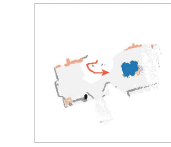


Figure 14. EPS Page2.

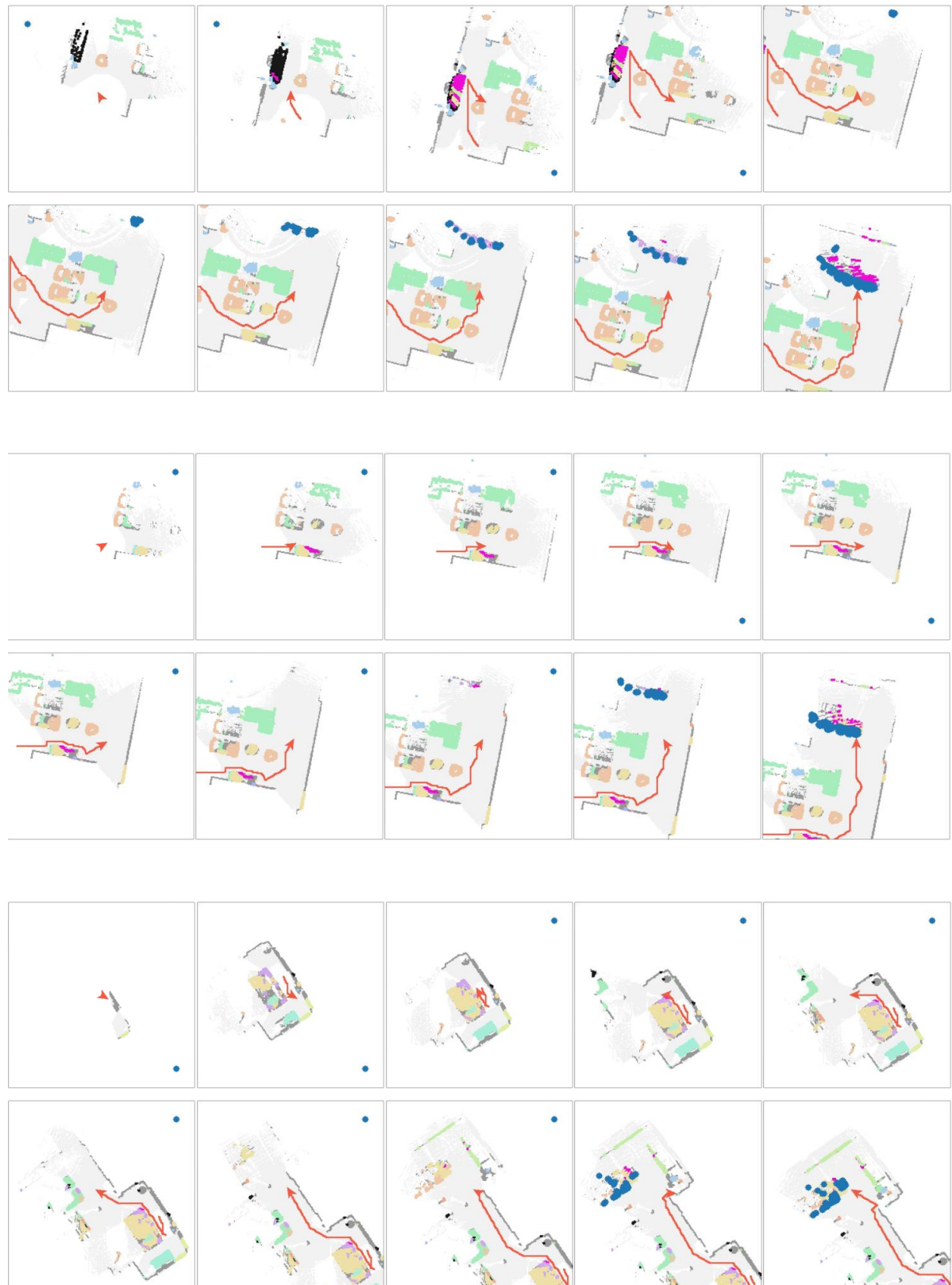


Figure 15. Episode results (1/3).



Figure 16. Episode results (2/3).



Figure 17. Episode results (3/3).